# Electronic Supplementary Information (ESI)

## Atomic-scale topochemical preparation of crystalline $Fe^{3+}$-doped β-$Ni(OH)_2$ for ultrahigh-rate oxygen evolution reaction

Kaiyue Zhu,[ab] Liu Huanying,[a] Mingrun Li,[a] Xuning Li,[bc] Junhu Wang,[c] Xuefeng Zhu*[a] and Weishen Yang[a]

[a] *State Key Laboratory of Catalysis, Dalian Institute of Chemical Physics. Chinese Academy of Sciences, Dalian 116023, P R China. E-mail: zhuxf@dicp.ac.cn; Fax: (+86) 411-84694447*

[b] *University of Chinese Academy of Sciences, Beijing, 100049, P R China*

[c] *Mössbauer Effect Data Center & Laboratory of Catalysts and New Materials for Aerospace, Dalian Institute of Chemical Physics, Chinese Academy of Sciences, Dalian 116023,P R China*

**Synthesis of $Fe^{3+}$-doped α-$Ni(OH)_2$ catalyst:**

$NiSO_4 \cdot 6H_2O$ (5 mmol) and $Fe_2(SO_4)_3 \cdot 4H_2O$ (2.5 mmol) were firstly dissolved into 20 mL deionized water with vigorous magnetic stirring, and then, $NiSO_4$/ $Fe_2(SO_4)_3$ mixed solution was added into the KOH solution (80 mL, 0.1 M) at a constant rate at 80 °C for 20 min. After that, the suspension was then kept stirring in air at 80 °C for another 5 h to synthesize $Fe^{3+}$-doped α-$Ni(OH)_2$ catalysts. After reaction finished, the precipitate was washed by deionized water and ethanol to remove residual ions and water, respectively. Finally, the product was dispersed into acetonitrile and then lyophilized.

**Synthesis of Fe-doped β-$Ni(OH)_2$ catalysts:**

For the preparation $Fe^{2+}$-doped β-$Ni(OH)_2$ precursor, $NiSO_4 \cdot 6H_2O$ (10(1-x) mmol, $0 \leq x \leq 1$) and $FeSO_4 \cdot 7H_2O$ (10x mmol) were firstly dissolved into 20 mL deionized water with vigorous magnetic stirring, and then, $NiSO_4$/$FeSO_4$ mixed solution was added into the KOH solution (80 mL, 0.1 M) at a constant rate under the protection of $N_2$ at 80 °C for 20 min. Dark green precipitation of $Fe^{2+}$-doped β-$Ni(OH)_2$ precursor was immediately produced. After that, the suspension was then exposed to air and kept stirring at 80 °C for another 5 h to synthesize $Fe^{3+}$-doped β-$Ni(OH)_2$ catalysts. The color of the precipitation changed from dark green to brown. After that, the precipitate was washed by deionized water and ethanol to remove residual ions and water, respectively. Finally, the product was dispersed into acetonitrile and then lyophilized to remove the solvent.

The commercial $IrO_2$ was obtained from Johnson Matthey Corp., which was tested as the benchmark in this paper.

**Material characterization:**

The XRD measurements were performed on Rigaku D/MAX 2500/PC with Cu Kα radiation (λ=0.154 nm at 40 kV and 200 mA). The data were recorded from 5º to 90º with an interval of 0.02º and a scan speed of 5º /min. The crystalline structures and elemental distribution maps of the Fe(0.5)-doped β-$Ni(OH)_2$ catalysts were acquired on a high

resolution transmission electron microscopy (HRTEM, FEI Tecnai F30) operated at 300 kV and an energy-dispersive X-ray spectrometer (EDS). Microscopic morphologies of the catalysts were observed on a scanning electron microscope (SEM, FEI Quanta 200 F). The infrared spectra were obtained at a Nicolet 6700 FTIR-ATR (Fourier Transform Infrared Spectroscopy -Attenuated Total Reflection) spectrophotometer. The information of surface chemical compositions and valence states of elements was collected by using an X-ray photoelectron spectroscopy (XPS, Thermo ESCALAB 250Xi) with Al Kα X-ray radiation (hυ =1486.6 eV). All the binding energy values were corrected by adventitious C 1s at 284.6 eV. The spectra were fitted by using the XPSPEAK41 software with Shirley-type background. The room temperature $^{57}$Fe Mössbauer spectra were recorded by proportional counter, and Topologic 500A spectrometer with $^{57}$Co (Rh) as a γ-ray radioactive source. Brunauer-Emmett-Teller (BET) surface area data were collected from a Quantachrome QUADRASORB SI instrument using physical adsorption at 77.3 K. Elemental analyses were also carried out with an inductively coupled plasma emission spectrometer (Shimadzu Corporation ICPS-8100). Fe impurity concentration of 78 ppb in 0.1 M KOH solution was determined by an inductively coupled plasma–mass spectrometry (ICP-MS, NexION 300D).

**Sample preparation for electrochemical characterizations:**

5 mg of catalyst and 5 mg Vulcan XC-72 were dispersed in a mixture solution of 2.00 mL isopropanol and 20 μL Nafion solution (5 wt%, Dupont, USA), and then the suspension was dispersed in an ultrasonic bath for about 30 min to form homogeneous ink. After that, 20 μL of the catalyst ink was loaded onto a glassy carbon electrode (Φ=5 mm) with a loading amount of 0.25 mg cm$^{-2}$, and then dried at room temperature. Before loading the catalyst, the glassy carbon electrode was polished with $Al_2O_3$ (0.05 μm) paste, followed by thoroughly washing with deioned water and then ethanol.

**Electrochemical characterizations:**

The measurements of cyclic voltammetry (CV), linear sweep voltammetry (LSV) and electrochemical impedance spectra (EIS) were performed in a conventional three-electrode electrochemical cell by using an electrochemical workstation based on a solartron 1287 electrochemical interface and a solartron 1260 frequency response analyzer. All the electrochemical measurements were performed on the rotating disk glassy carbon with loaded catalyst as working electrode, saturated calomel electrode (SCE) as the reference electrode and platinum wire as counter electrode in 0.1 M KOH solution. Measurements were calibrated with respected to reversible hydrogen electrode (RHE).

Firstly, the OER polarization curves were recorded by LSV at a scan rate of 10 mV $s^{-1}$ in $O_2$-saturated 0.1 M KOH with a rotating speed of 1600 rpm. The stability tests were performed in $O_2$-saturated 0.1 M KOH by galvanostatic test at 10 mA $cm^{-2}$. The potential values were iR-corrected to eliminate the effect of solution resistance, which were calculated by the following equation: $E_{iR\text{-}corrected}=E\text{-}iR$, where i is the current, and R is the ohmic resistance of electrolyte measured via high frequency ac impedance in $O_2$-saturated 0.1 M KOH. Impedance spectra were measured in a frequency range of $10^{-2}$ Hz –$10^5$ Hz at five points per frequency decade with amplitude of 10 mV.

To compare with other works, we calibrated the reference electrode with respect to reversible hydrogen electrode (RHE). The RHE calibration was carried out in $H_2$-saturated 0.1 M KOH solution with platinum wire as the working electrode. The cyclic voltammetry was performed near the thermodynamic potential for the $H^+/H_2$ reaction at a scan rate of 1 mV $s^{-1}$. The average of the two potentials at which the current passed through zero was treated as the potential of the hydrogen electrode reaction. $E_{RHE}=E_{SCE}+1.0052$ V.

The electrical double layer capacitance ($C_{dl}$) was measured from double-layer charging curves from the scan-rate dependence of cyclic voltammetric stripping. Working electrodes were scanned from -0.15 V to -0.05 V versus SCE (0.1M KOH) for several potential cycles until the signals were stabilized, and the CV data were collected. The scan rates were 10 mv $s^{-}$

$^{1}$, 20 mv $s^{-1}$, 40 mv $s^{-1}$, 60 mv $s^{-1}$, 80 mV $s^{-1}$ and 100 mV $s^{-1}$. The $C_{dl}$ was estimated by plotting the $\Delta j=(j_a-j_c)$ (where $j_a$ and $j_c$ are the anodic and cathodic current densities, respectively) against the scan rate, and the slope is twice that of $C_{dl}$.

**Methods**

The binding energy calculations were performed based on the Kohn-Sham formalism of density-functional theory as implemented in the Vienna ab initio package[1,2]. The generalized gradient approximation Perdew-Burke-Ernzerhof exchange-correlation functional was employed[3]. The projector augmented wave method was applied to describe the interaction between the ions and electrons ("ion" refers to a nucleus screened by its core electrons).[4] The total energies and Hellmann-Feynman forces acting on atoms were converged below $10^{-3}$ eV per atom and 0.1 eV $Å^{-1}$, respectively. The vacuum thickness was set to above 20 Å for slab model, which is enough to avoid the interaction between layers.

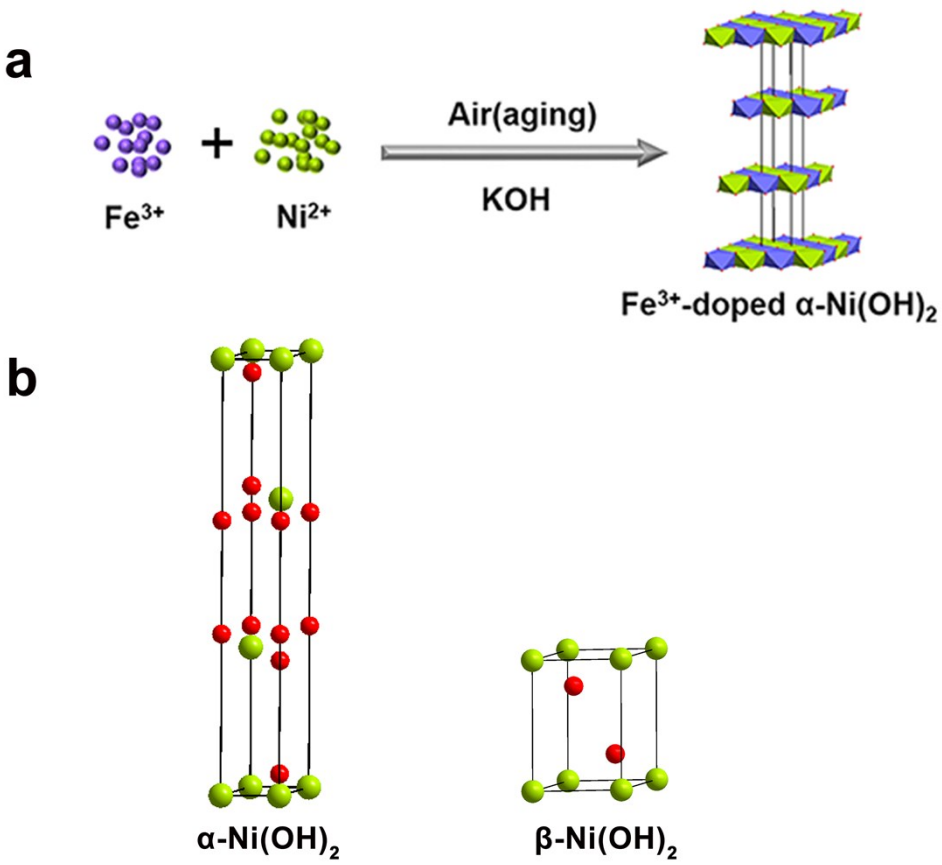


**Fig. S1.** (a) Schematic illustrations of the synthesis of $Fe^{3+}$-doped α-$Ni(OH)_2$ sample. (b) The crystal structures of α-$Ni(OH)_2$ and β-$Ni(OH)_2$. For the α-$Ni(OH)_2$ (space group R-3m) and β-$Ni(OH)_2$ (space group P-3m1), the distance of Ni-Ni in [NiO6] layers is the same, while the distance of Ni-Ni between [NiO6] layers is different. The arrangements of cations in crystal structures are just for models.

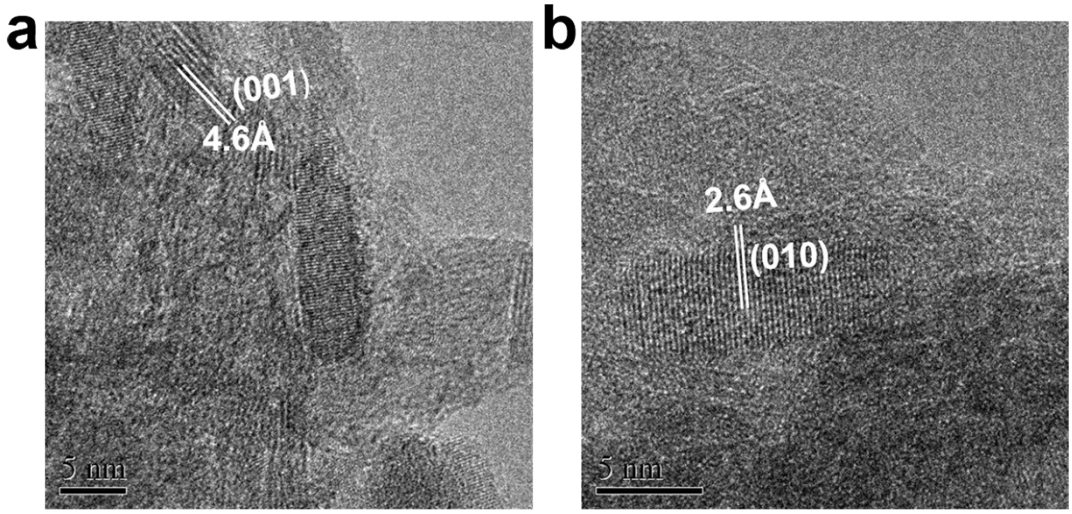


**Fig. S2.** (a) and (b) HRTEM images of Fe(0.5)-doped β-$Ni(OH)_2$ samples.

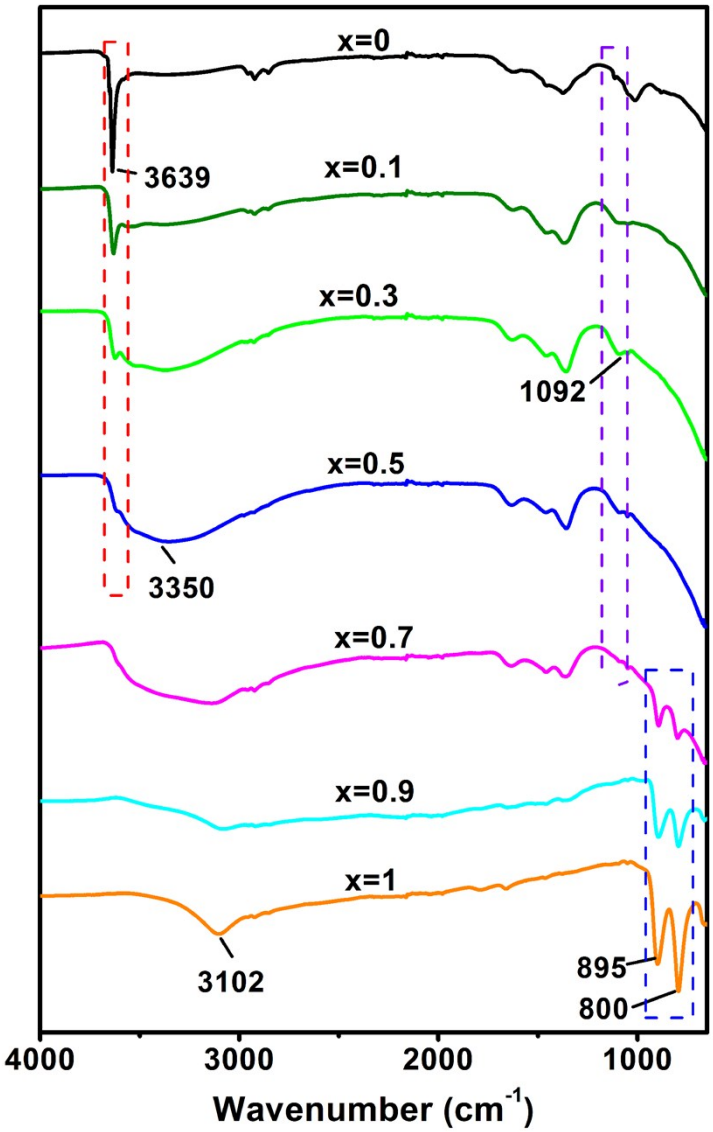


**Fig. S3.** The attenuated total reflection infrared spectra of the Fe-doped $Ni(OH)_2$ with various Fe contents

A narrow and sharp peak at 3639$cm^{-1}$ is owing to the stretching vibration of non-hydrogen bonded hydroxyl, which confirms the β-$Ni(OH)_2$ phase of the product.[5,6] The absorbance of this band decreased and the band is broadened by a shoulder at 3350 $cm^{-1}$ with increasing amount of doped iron, but this band appeared even when doped with 50% Fe, indicating that the Ni ions were replaced by $Fe^{3+}$ ions. The band at 1092 $cm^{-1}$ was attributed to Fe-O-H bending vibration of Fe-doped β-$Ni(OH)_2$ samples.[7] As doping amount of iron above 0.5, the peak appeared at 895 $cm^{-1}$ and 800$cm^{-1}$ can be well assigned to α-FeOOH.[8]

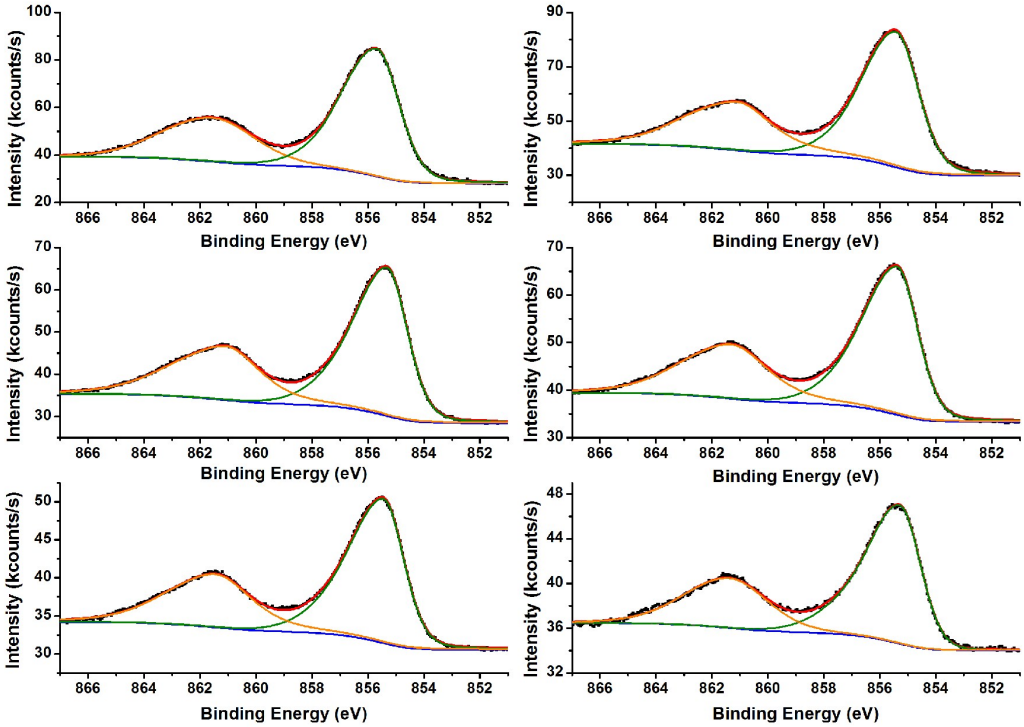


**Fig. S4.** Ni $2p_{3/2}$ XPS spectra of as-prepared Fe-doped $Ni(OH)_2$ with various Fe contents. The Ni $2p_{3/2}$ XPS spectra can be well fitted with two peaks. The peak with binding energy located at ~533.4 eV is assigned to the $Ni^{2+}$ species on the surface, whereas the other peak with binding energy located at ~861.3 eV is attributed to the satellite peak.[9]

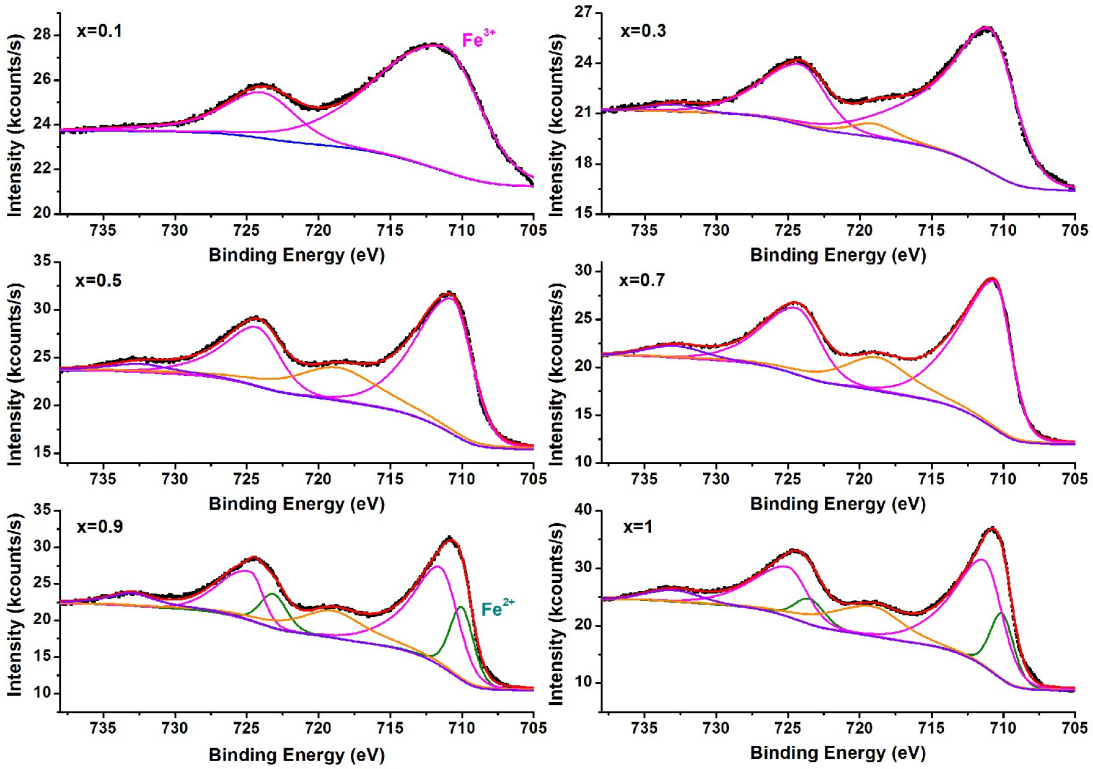


**Fig. S5.** Fe 2p XPS spectra of as-prepared Fe-doped $Ni(OH)_2$ with various Fe contents. A spin−orbit doublet of Fe2$p_{1/2}$ and Fe2$p_{3/2}$ with a binding energy gap of ~13.5 eV forms the Fe 2*p* spectra. Two peaks with binding energy located at 710.0 and 711.3 eV are assigned to the $Fe^{2+}$ and $Fe^{3+}$, respectively. Fe 2p XPS spectra of Fe(x≤0.7)-doped $Ni(OH)_2$ indicates that the Fe oxidation state is predominantly +3, while Fe 2p XPS spectra of Fe(x=0.9,1)-doped $Ni(OH)_2$ show the possible existence of $Fe^{3+}$ and $Fe^{2+}$ due to the formation of $Fe_3O_4$.[10]

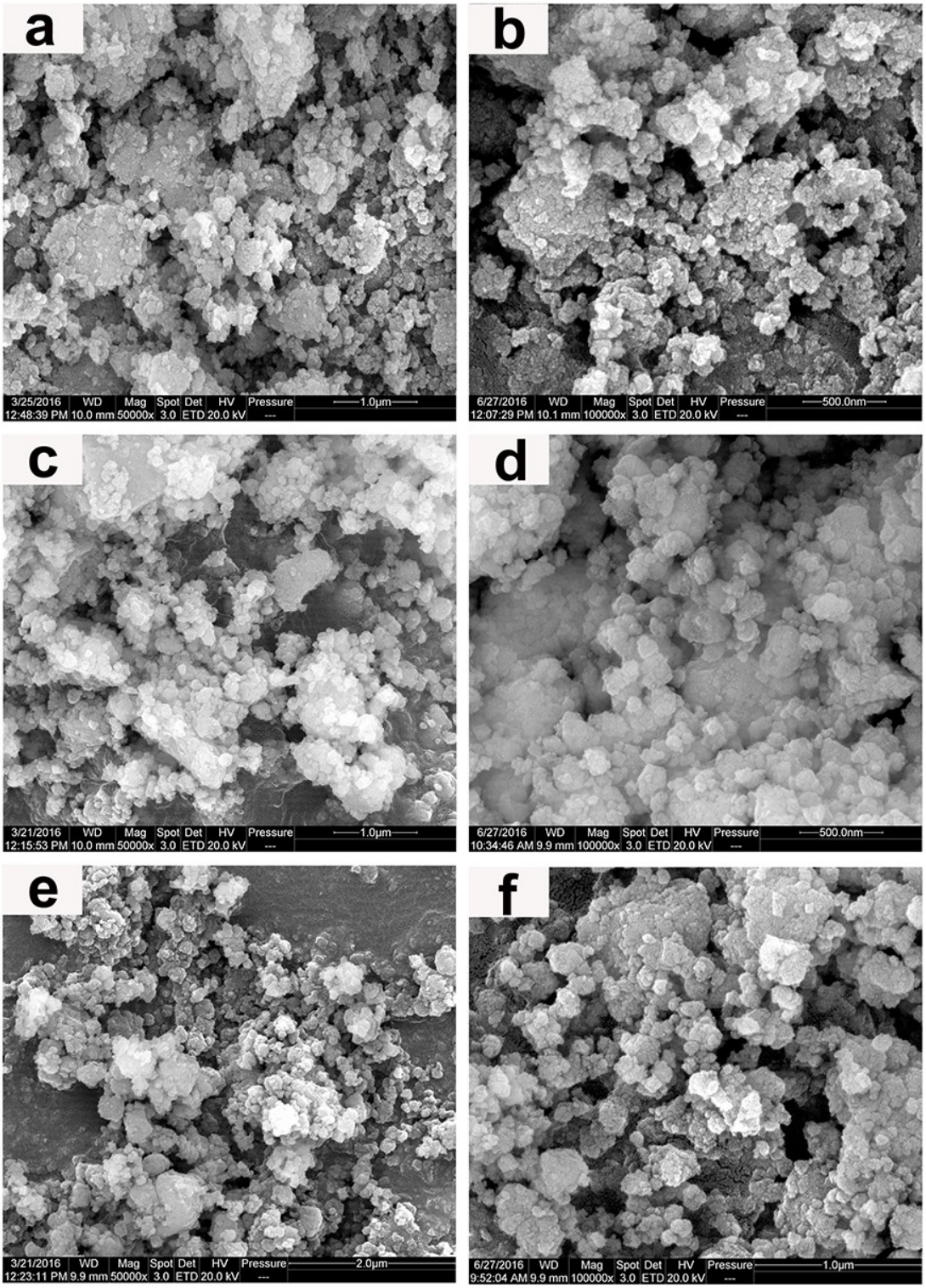


**Fig. S6.** SEM images of Fe-doped $Ni(OH)_2$ with various Fe contents. (a and b) x=0, (c and d) x=0.1 and (e and f) x=0.3.

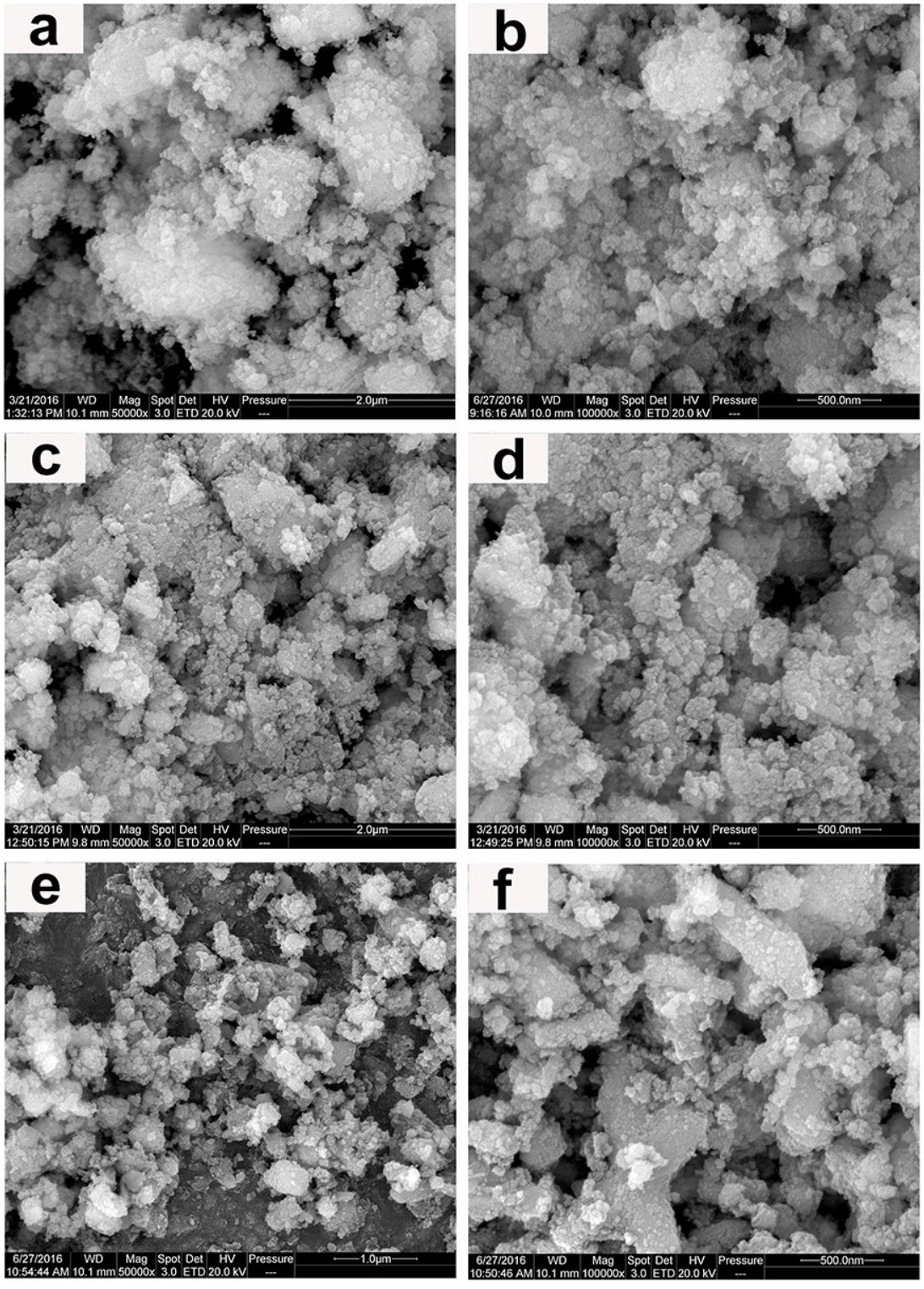


**Fig. S7.** SEM images of Fe-doped $Ni(OH)_2$ with various Fe contents. (a and b) x=0.5, (c and d) x=0.7 and (e and f) x=0.9.

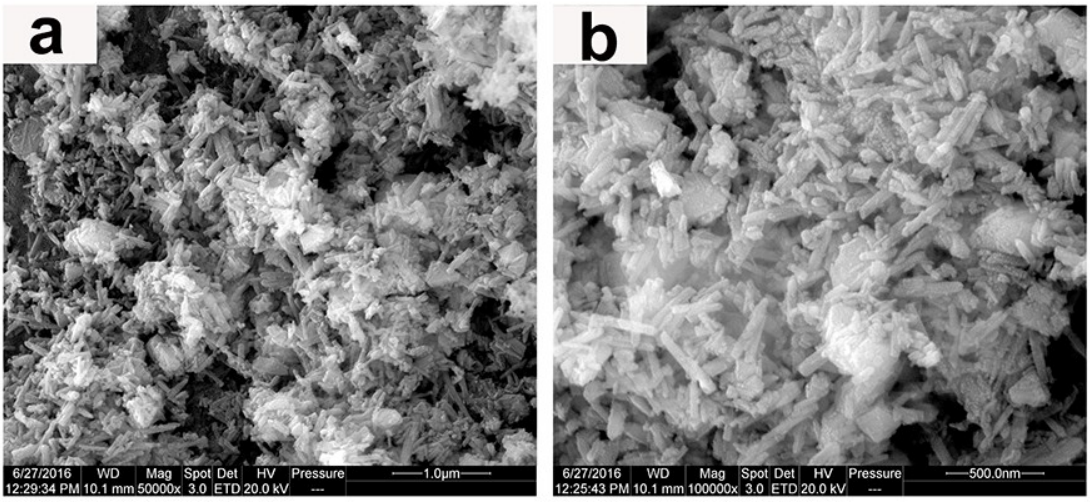


**Fig. S8.** SEM images of Fe(x=1)-doped $Ni(OH)_2$ powders.

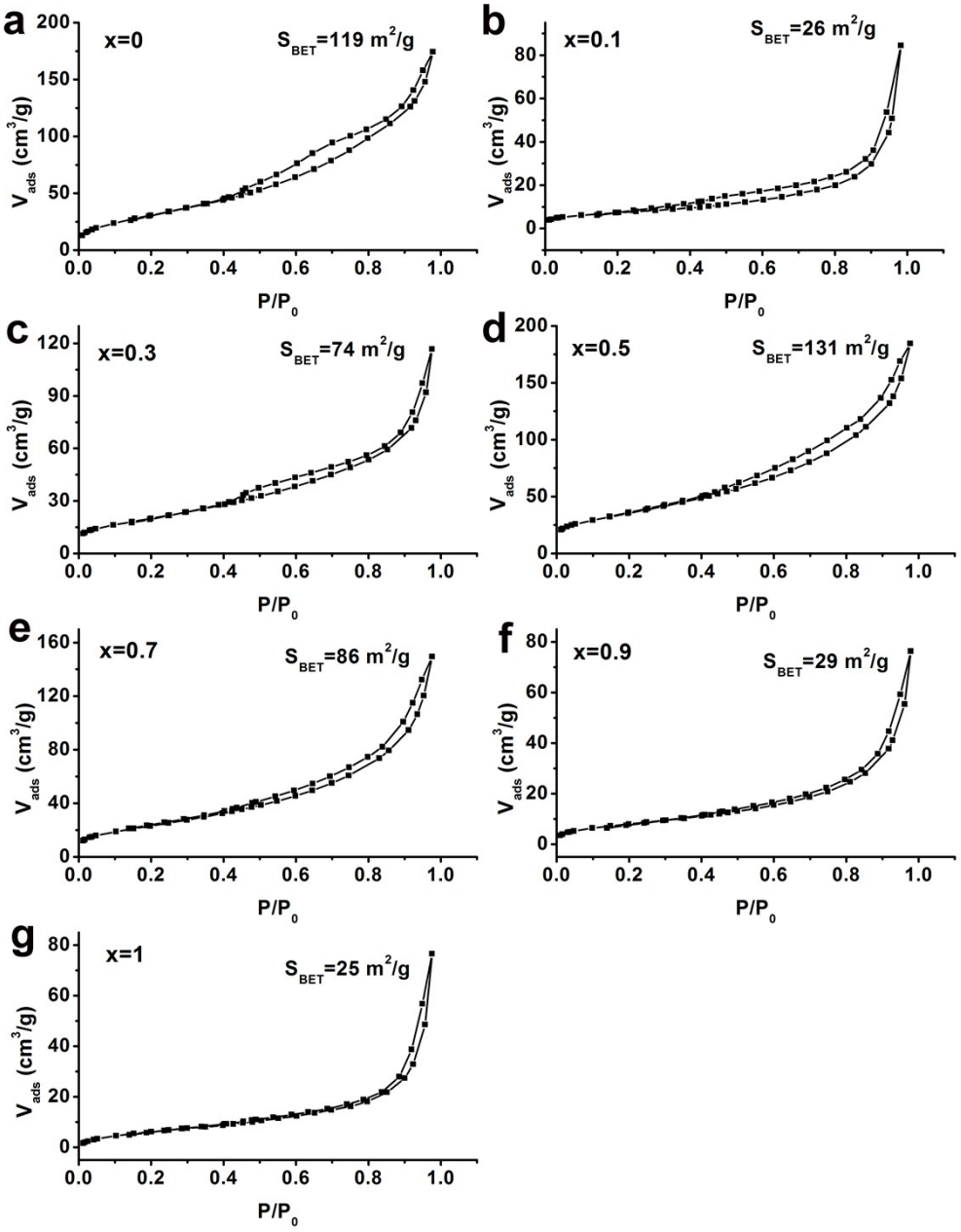


**Fig. S9.** Nitrogen adsorption-desorption isotherm curves of Fe-doped $Ni(OH)_2$ catalysts with various Fe contents.

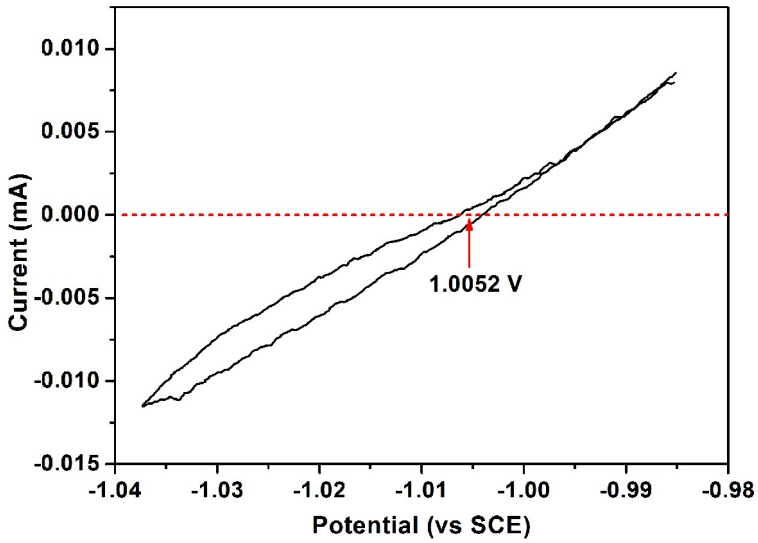


**Fig. S10.** Potential calibration of the reference electrode in $H_2$-saturated 0.1 M KOH solution. The potentials were calculated by the equation: $E_{RHE}=E_{SCE}+1.0052$ V.

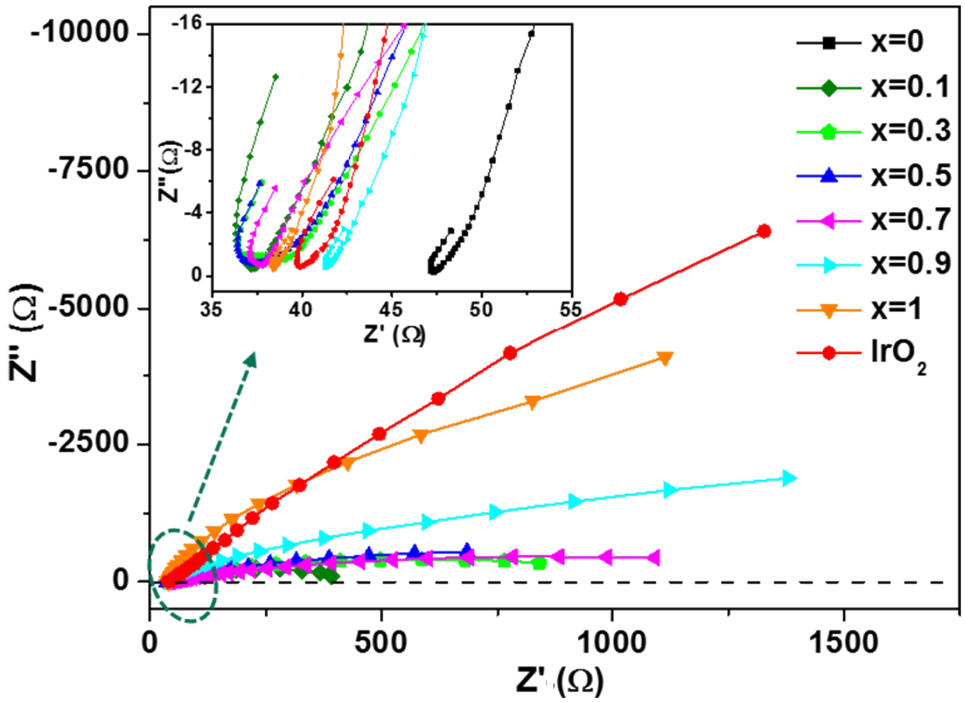


**Fig. S11.** Impedance spectra of Fe-doped $Ni(OH)_2$ catalysts and the commercial $IrO_2$ under open circuit conditions. The inserted figure is the partial enlargement drawing of elliptic region.

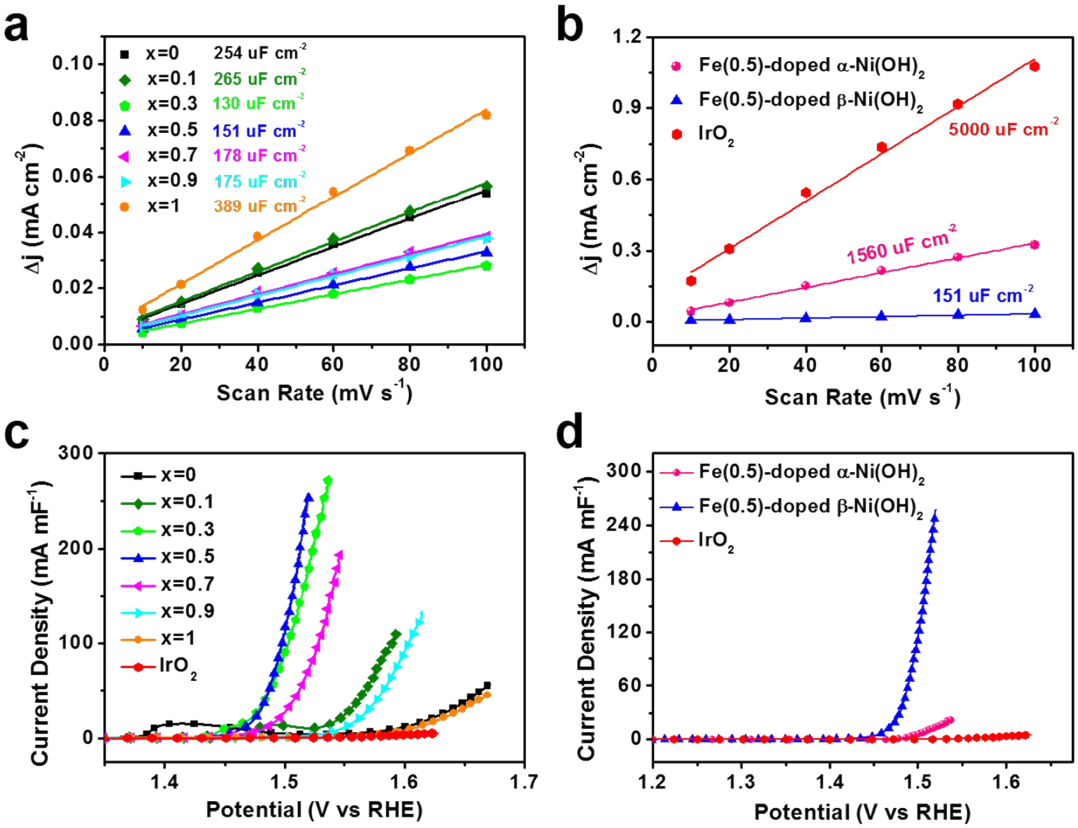


**Fig. S12.** Plots of charging current density differences Δj *vs* the scan rate for (a) Fe-doped $Ni(OH)_2$ catalysts with various Fe contents and (b) Fe(0.5)-doped α-$Ni(OH)_2$, Fe(0.5)-doped β-$Ni(OH)_2$ and $IrO_2$. OER activities normalized by electrical double layer capacitance for (c) Fe-doped $Ni(OH)_2$ catalysts with various Fe contents and (d) Fe(0.5)-doped α-$Ni(OH)_2$, Fe(0.5)-doped β-$Ni(OH)_2$ and $IrO_2$. As Fe contents increasing, the changing trend of the OER activities normalized by the $C_{dl}$ is consistent with that normalized by the glassy carbon disk area, except the values are different.

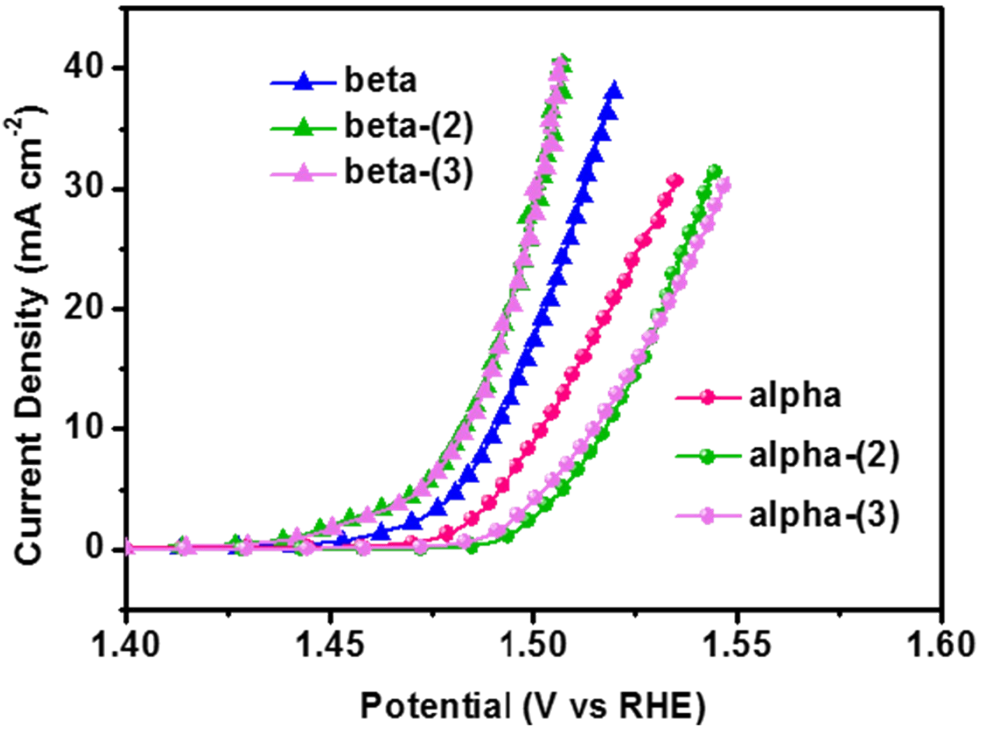


**Fig. S13.** OER performance of Fe(0.5)-doped α-$Ni(OH)_2$ and Fe(0.5)-doped β-$Ni(OH)_2$. The linear sweep voltammetry (LSV) measurements for Fe(0.5)-doped α-$Ni(OH)_2$ and Fe(0.5)-doped β-$Ni(OH)_2$ were repeated for three times, the best performance (red sphere line) of Fe(0.5)-doped α-$Ni(OH)_2$ was taken to compare with the worst performance (blue triangle line) of Fe(0.5)-doped β-$Ni(OH)_2$. The 12 mV difference in overpotential at 10 mA $cm^{-2}$ is the minimal difference in our experiments, so the difference should not be ignored.

**Table S1.** Compositions of various species on Fe-doped $Ni(OH)_2$ catalysts from inductively coupled plasma-atomic emission spectrometry (ICP-AES).

| Catalysts | Fe/(Ni+Fe) |
|---|---|
| x=0 | 0 |
| x=0.1 | 0.102 |
| x=0.3 | 0.303 |
| x=0.5 | 0.498 |
| x=0.7 | 0.701 |
| x=0.9 | 0.921 |
| x=1 | 1 |

**Table S2.** The parameters of the fitted curves to the Mössbauer spectra of the Fe-doped $Ni(OH)_2$ catalysts.

| Catalysts | Assignment | IS (mm $s^{-1}$) | QS (mm $s^{-1}$) | $B_{hf}$ (T) | Γ (mm $s^{-1}$) | Area (%) |
|---|---|---|---|---|---|---|
| x=0.1 | Super-FeOOH | 0.33 | 0.71 | | 0.55 | 100 |
| x=0.3 | Super-FeOOH | 0.36 | 0.73 | | 0.47 | 100 |
| x=0.5 | Super-FeOOH | 0.34 | 0.69 | | 0.44 | 100 |
| x=0.7 | α-FeOOH | 0.37 | -0.29 | 38 | 0.61 | 31 |
| | Super-FeOOH | 0.34 | 0.69 | | 0.47 | 69 |
| x=0.9 | A-site Fe of $Fe_3O_4$ & $Fe_2O_3$ | 0.29 | 0.01 | 49.1 | 0.41 | 23 |
| | B-site Fe of $Fe_3O_4$ | 0.63 | -0.07 | 46.1 | 0.47 | 23 |
| | α-FeOOH | 0.38 | -0.27 | 37.6 | 0.54 | 36 |
| | Super-FeOOH | 0.35 | 0.72 | - | 0.48 | 18 |
| x=1 | A-site Fe of $Fe_3O_4$ & $Fe_2O_3$ | 0.26 | 0.04 | 49.2 | 0.36 | 17 |
| | B-site Fe of $Fe_3O_4$ | 0.58 | -0.18 | 46.2 | 0.47 | 15 |
| | Super-FeOOH | 0.35 | -0.28 | 37.6 | 0.54 | 68 |

**Table S3.** Ni 2p and Fe 2p XPS fitting data for the as-synthesized Fe-doped $Ni(OH)_2$ samples.

| Catalysts | Ni2p | | Fe2p | | | | | | Fe/(Ni+Fe) |
|---|---|---|---|---|---|---|---|---|---|
| | Ni2p3/2 | S1[a] | Fe2p3/2 | | S2[a] | Fe2p1/2 | | S3[a] | |
| x=0 | 855.6 | 861.5 | | | | | | | 0 |
| x=0.1 | 855.4 | 861.1 | 711.2 | | | 723.9 | | | 0.336 |
| x=0.3 | 855.3 | 861.1 | 711.0 | | 719.0 | 724.1 | | 733.0 | 0.444 |
| x=0.5 | 855.4 | 861.3 | 710.7 | | 718.6 | 724.2 | | 732.4 | 0.520 |
| x=0.7 | 855.3 | 861.1 | 711.0 | | 719.0 | 724.1 | | 733.0 | 0.649 |
| x=0.9 | 855.3 | 861.4 | 711.5 | 710.0 | 719.0 | 724.7 | 723.1 | 733.0 | 0.738 |
| x=1 | | | 711.3 | 710.1 | 719.0 | 724.7 | 723.5 | 733.0 | 1 |

[a]S1 is the satellite peak of Ni 2p; both S2 and S3 are the satellite peaks of Fe 2p.

**Table S4** BET surface areas of Fe-doped $Ni(OH)_2$ catalysts.

| Catalysts | Area ($m^2/g$) |
|---|---|
| x=0 | 118 |
| x=0.1 | 26 |
| x=0.3 | 74 |
| x=0.5 | 131 |
| x=0.7 | 86 |
| x=0.9 | 29 |
| x=1 | 25 |

**Table S5.** OER activities of some benchmark catalysts in alkaline solution.

| Catalysts | Electrolytes | η(V)@10 mA $cm^{-2}$ | Tafel slope (mV $dec^{-1}$) | Working Conditions | References |
|---|---|---|---|---|---|
| Fe(0.5) doped β-$Ni(OH)_2$ | 0.1 M KOH | 0.26 | 32 | 0.25 mg $cm^{-2}$ on GCE (ϕ=5mm) | This work |
| $IrO_2$ | 0.1 M KOH | 0.34 | 85 | 0.25 mg $cm^{-2}$ on GCE (ϕ=5mm) | This work |
| NiFe-LDH/CNT | 0.1 M KOH | 0.31 | 35 | 0.2 mg $cm^{-2}$ on GCE (ϕ=5mm) | 24 |
| $Ba_{0.5}Sr_{0.5}Co_{0.8}Fe_{0.2}O_{3-\delta}$ | 0.1 M KOH | 0.51 | 94 | 0.23 mg $cm^{-2}$ on GCE (ϕ=5mm) | 40 |
| $Co_3O_4$/N-rmGO | 1 M KOH | 0.31 | 67 | 1 mg $cm^{-2}$ on Ni foam | 41 |
| α-$Ni(OH)_2$ | 0.1 M KOH | 0.33 | 42 | 0.2 mg $cm^{-2}$ on GCE (ϕ=5mm) | 3 |
| G/$Ni_{0.44}Fe_{0.56}$-LDH | 0.1 M KOH | 0.39 | 67 | 0.25 mg $cm^{-2}$ on GCE (ϕ=5mm) | 30 |
| amorphous $Ni_{0.71}Fe_{0.29}(OH)_x$[11] | 0.1 M KOH | 0.30 | 58 | 0.31 mg $cm^{-2}$ on the graphite electrode | S11 |
| Ni-$Fe_{0.52}$ LDH | 1 M KOH | 0.34 | 97 | 0.14 mg $cm^{-2}$ on GCE (ϕ=3mm) | 23 |
| $SrNb_{0.1}Co_{0.7}Fe_{0.2}O_{3-\delta}$ | 0.1 M KOH | 0.50 | 76 | 0.23 mg $cm^{-2}$ on GCE (ϕ=5mm) | 40 |

Note: NiFe-LDH/CNT is ultrathin nickel-iron layered doble hydroxide (LDH) nanoplates on mildly oxidized multiwalled carbon nanotubes (CNT)

## REFERENCES


1 G. Kresse and J. Furthmüller, *Phys. Rev. B* 1996, **54**, 11169.

2 G. Kresse and J. Furthmüller, *Comp. Mater. Sci.*, 1996, **6**, 15.

3 J. Perdew, K. Burke and M. Ernzerhof, *Phys. Rev. Lett.*, 1996, **77**, 3865.

4 P. Blochl, *Phys. Rev. B: Condens. Matter*, 1994, **50**, 17953.

5 B. Li, M. Ai and Z. Xu, *Chem. Commun.*, 2010, **46**, 6267.

6 C. Greaves and M. A. Thomas, *Acta Cryst.*, 1986, **42**, 51.

7 P. Chen, K. Xu, X. Li, Y. Guo, D. Zhou, J. Zhao, X. Wu, C. Wu and Y. Xie, *Chem. Sci.*, 2014, **5**, 2251.

8 S. Rahimi, R. M. Moattari, L. Rajabi, A. A. Derakhshan and M. Keyhani, *J. Ind. Eng. Chem.*, 2015, **23**, 33.

9 S. Chou, F. Cheng and J. Chen, *Eur. J. Inorg. Chem.*, 2005, 4035.

10 A. P. Grosvenor, B. A. Kobe, M. C. Biesinger and N. S. McIntyre, *Surf. Interface Anal.*, 2004, **36**, 1564.

11 Y. Gao, X. Liu and G. Yang, *Nanoscale*, 2016, **8**, 5015.